Chemistry Africa (2022) 5:2259–2269
https://doi.org/10.1007/s42250-022-00469-3

ORIGINAL ARTICLE

Multi-walled Carbon Nanotube/Acrylonitrile Butadiene Styrene Nanocomposite Filaments for Fused Deposition Modelling Type 3D Printing

Serhat Oran[1,2] · Hatice Aylin Karahan Toprakci[1] · Ozan Toprakci[1] · Mehmet Atilla Tasdelen[1]

Received: 31 May 2022 / Accepted: 29 August 2022 / Published online: 21 September 2022

Abstract
The multi-walled carbon nanotube/acrylonitrile-butadiene-styrene (MWCNT/ABS) nanocomposite filaments containing 3, 5, and 10 wt% nanofiller were prepared by an extruder to use the fused deposition modeling (FDM) type three-dimensional (3D) printing technique. The functional MWCNT/ABS nanocomposites were converted into monofilament form by a special extrusion die. In the next step, test samples were produced from the obtained nanocomposite filaments on FDM printers to characterize morphological, electrical, and mechanical properties. As a result of characterization tests, the optimum 3D printing temperature and loading ratio of MWCNT are determined as 250 °C and 10 wt%, respectively. This sample, which has the lowest volume resistivity as 2.13E7 ohm.cm, meets the requirements of electrostatic discharge materials. The presence of MWCNT in ABS matrix resulted in a significant improvement in elastic modulus and thermal properties, but a decrease in elongation at break and impact strength. In this study, it was revealed that the MWCNT nanofiller in ABS matrix can change the morphology of the 3D printed sample as foam-like porous structures, which possibly leads to reduced resistance to stress.

Keywords additive manufacturing · 3D printing · electrical properties · monofilament · fused deposition modelling · nanocomposites

1 Introduction

Additive manufacturing technology, known as three-dimensional (3D) printing, has been developing since the 90s and is mostly used to produce prototypes of elements in complex geometries [1, 2]. The 3D printing technology is a new generation production technique that enables the layered production of three-dimensional objects designed by computer aided design (CAD) programs on the computer [3]. Today, fused deposition modeling (FDM) technology, in which thermoplastics are used, has a 69% share in the current 3D printing market. This technology has begun to be employed in many fields such as biomedicine[4, 5], fashion[6, 7], construction[8], space and aviation[9], automotive, and electronics, etc. [10, 11]. Compared to other 3D printing techniques, it offers unique advantages such as conceptually simple installation, inexpensive device and operating costs, clean, and easy to use even at home, acceptable mechanical performance, and good surface quality, thanks to its convenience in producing and modifying parts. The FDM technique is a filament-based production process and based on the method of storing thermoplastic materials layer by layer on the bed surface (glass, metal, epoxy, etc.) by melting them through a hot nozzle. It simply enables the production of 3D objects at different layer thicknesses, filling ratios, speeds, and temperatures with nozzle and table movements in three-dimensional axes. Furthermore, many thermoplastics including acrylonitrile-butadiene-styrene terpolymer (ABS), poly(lactic acid) (PLA), and modified poly(ethylene terephthalate glycol) (PETG) are used in FDM technology [12]. Polymer viscosity, melt temperature, heat capacity, thermal conductivity, printing orientation,

✉ Mehmet Atilla Tasdelen
tasdelen@yalova.edu.tr

[1] Department of Polymer Materials Engineering, Faculty of Engineering, Yalova University, Yalova, Turkey

[2] Department of Polymer Materials Engineering, Institute of Graduate Studies, Yalova University, Yalova, Turkey

cooling rate, raster angle, raster width, layer height, and air gap are some important parameters in the FDM technique. While there is no need for a closed cabinet during the 3D printing of PLA and PETG filaments, ABS and some other thermoplastics require closed-type 3D printers due to their rheological behavior. In addition, the mechanical performance of printed parts is restricted by weak interlamination between partially liquefied filaments and preprinted layers. At this point, the optimization of 3D printing parameters such as layer height, printing speed, cooling rate, and orientation is frequently applied in practice, however, this way brings limited improvements in the mechanical properties of printed materials [13–15].

Until now, many researchers have continued to work on improving the mechanical, chemical, thermal, and electrical properties of the 3D printed materials as well as giving them additional functionalities [16, 17]. Currently, the most practical method to improve the properties of 3D printed materials is the use of nanofillers, which not only provide a reinforcing function but also act as active ingredients in the thermoplastic matrix [18]. Due to the large surface area that lead to significant interphase or boundary area between the thermoplastic matrix and nanofillers; nanocomposite filaments can contribute to improvement of mechanical, thermal, and other physical properties of 3D printed materials [19–22]. For example, with the homogenous dispersion of carbon-based nanofillers such as carbon black, graphene oxide, graphene, and carbon nanotube (CNT) [23–28] in the thermoplastic filaments, the 3D printed parts can be used in many fields including electronic sensors, circuits, microbatteries, electromagnetic shielding (EMI), and electrostatic discharge (ESD) applications based on their electrical properties [29–32]. Due to the excellent mechanical, electrical, and thermal conductivity properties of CNT, it has been used as a reinforcing agent to produce functional nanocomposites [33–36]. In addition to its unique properties, its lightweight structure and ability to increase mechanical strength and electrical conductivity make it an ideal nanofiller for polymer nanocomposites. Based on the number of graphene cylinders, the CNT is classified as single-walled CNT (SWCNT) containing only one graphene layer and multi-walled CNT (MWCNT) having many graphene layers [37]. Compared to the SWCNT, the MWCNT has lower price, better availability, higher conductivity, and easier production. All these, make it an attractive nanofiller for the fabrication of polymer nanocomposites [38–40].

In this study, the effects of MWCNT as a functional filler on the mechanical and electrical properties of ABS thermoplastic matrix was intensively investigated for the FDM type 3D printing technique. In the literature, polymer nanocomposites having an electrical resistivity range between 10^6 and 10^{12} ohm.cm can be employed in ESD protection applications.[32] For this purpose, the MWCNT/ABS nanocomposites were produced by a coaxial twin screw extruder by mixing various amounts of MWCNT (3, 5, and 10 wt%) into the ABS matrix. The obtained nanocomposites were converted into filament form by an industrial type of monofilament production line, and then these filaments were printed with an FDM type 3D printer to produce test samples for the mechanical, electrical, and morphology analyses. Hence, this study was intended to develop 3D printed MWCNT/ABS nanocomposites with the combination of acceptable mechanical and electrical properties that could be used in ESD applications.

2 Experimental

2.1 Materials

The high impact ABS polymer was purchased from the Sabic Company (Saudi Arabia) with the code EX58F. The pristine MWCNT without any surface modification (purity > 95%) was supplied by Nanografi Company (Turkey). Based on the technical data sheet, the outer diameter, inside diameter and length of the MWCNT were 30–50 nm, 5–10 nm, and 10–25 µm, respectively. As given in Fig.S6, outer tube diameter was determined as 37.5 nm that is in the range of the company information. The aspect ratio of MWCNT was reported to be between 200 and 833 based on given nanotube dimensions.

2.2 Nanocomposite Production and Filament Extrusion

A coaxial twin-screw extruder with a screw diameter of 16 mm and an L/D ratio of 25 was used to homogeneously distribute the MWCNT nanofillers into the polymer matrix at different ratios. Both ABS and MWCNT were dried at 80 °C for 4 h and dried mixed before feeding into the extruder. Using the melt mixing method, the MWCNT was mixed with ABS polymer matrix at 3, 5, and 10% weight ratios. In the extrusion process, the temperature profile from the feeding zone to the extruder die were determined as $T_1 = 180$ °C, $T_2 = 205$ °C, $T_3 = 210$ °C, $T_4 = 220$ °C and $T_5 = 230$ °C, respectively. Polymer nanocomposites were extruded in the form of granules and made ready for filament production (Table 1).

The nanocomposite granules were converted to filament form by an industrial type of monofilament production line to be used in FDM type printers. The granules were dried at 80 °C for 4 h before the process. The temperature profile from the feeding zone to the extruder die were determined as 200/220/220/230/240/250/255°C, respectively. To

Table 1 Sample codes, contents and 3D printing conditions

Sample code	Filler content (wt%)	3D printing temperature (ºC)
C0-250	0	250
C3-250	3	250
C5-250	5	250
C10-230	10	230
C10-250	10	250
C10-260	10	260
C10-270	10	270

produce mechanical, morphological, and conductivity test specimens by a 3D printer, 270 m long 750 gr MWCNT/ABS nanocomposite filaments were produced (Fig. S1). In FDM-type 3D printing technology, the extruded filaments should provide high diameter precision and the lowest ovality, which are critical points for printed parts to have higher mechanical performance and good surface finish. It was observed that the extrusion speed directly affected the filament diameter during filament extrusion. The MWCNT/ABS nanocomposite materials prepared with nanofiller at different ratios were brought into filament form with a diameter of 1.75 mm (with a tolerance of ± 0.05 mm) in the industrial type of monofilament production line.

2.3 Preparation of Test Specimens by 3D Printing

A Zaxe X1 brand 3D printer with an FDM type closed cabinet was used to print test samples from nanocomposite filaments (Fig. S2-4). While the mechanical test samples were prepared according to international standards, the imprinted test sample was specially designed for electrical conductivity measurements and conductivity test system. The tensile test specimen was prepared according to ASTM D638 Type I standard dog bone test specimen dimensions ($3 \times 20 \times 165$ mm; thickness (t), width (w), length (l), respectively) (Fig. S2). The impact test specimen ($4 \times 10 \times 80$ mm; t, w, l, respectively) (Fig. S3) was notched according to ASTM D-256 test specimen standards. In addition, the test samples for the volume resistivity measurement had a wall thickness of 1 mm and a radius (r) of 45 mm (Fig. S4). The test samples designed in the 3D CAD program were converted to *gcode format in the Zaxe slicing program. In the slicing program, printing parameters such as printing and table temperatures, and layer thickness were kept constant for mechanical and morphology analysis. Nozzle temperature was set as 255 °C and the table temperature was kept constant at 100 °C according to the glass transition temperature (T_g) of ABS. The thickness of each layer was determined as 0.2 mm, and the samples were produced with a 100% infill density by the 3D printer [41]. The nozzle diameter was 0.4 mm, that is the standard size for desk-type FDM printers. To obtain accurate mechanical and resistivity results, all test samples were kept at standard laboratory conditions (at 25–26 °C, under 65% RH) for 20 h before the tests. Parameters of the 3D printing were summarized in Table 2.

Table 2 Printing parameters of test samples in FDM type 3D printer

Printing parameters	Value	Unit
Printing speed	50	mm/s
Nozzle diameter	0.4	mm
Nozzle temperature	255	°C
Bed temperature	100	°C
Infill density	100	%
Layer height	0.2	mm
Cooling after print	r.t.*	°C
Filament diameter	1.75	mm
Test temperature	r.t.*	°C
Cooling time	2	h
Sample print plane	X,Y –Axis	-

*r.t.: room temperature

2.4 Melt Flow Index (MFI) Analysis

The melt flow index (MFI) is a practical test method for the simple investigation of the rheological behavior of polymers. In FDM technology, the melt flow behavior of thermoplastics is a crucial parameter for optimizing 3D printing parameters. For this analysis, the nanocomposite filaments were cut into small pieces and fed into the MFI test device. The MFI measurements were carried out at 220 °C with an applied load of 10 kg by using a Ceast MF20 model (die length of 8.000 mm and die diameter of 2.096 mm) following ISO 1133 standard. The average values of five measurements were recorded, average and standard deviation (SD) values were depicted in the graph.

2.5 Morphological Characterization

Morphology of nanocomposites was studied by using a scanning electron microscope (SEM). The conductivity test samples were fractured in liquid nitrogen and the fracture surfaces were observed at an acceleration voltage of 25 kV (FEI Inc., Inspect S50 SEM). Samples were sputter coated (Au/Pd alloy, 3–6 nm) before the analysis. Representative micrographs of the 3D-printed ABS and 3, 5, and 10 wt % of MWCNT filled nanocomposites at various magnifications were selected.

2.6 Characterization of Volume Resistivity

The Keithley 8009 resistivity meter was used to measure the volume and surface resistance of materials. The device could measure direct current resistance or resistivity of materials based on ASTM D257 test standards. Samples (t:

1 mm, r: 45 mm) were prepared according to the electrode dimensions of the test device. The average of five measurements and corresponding standard deviation (SD) values were calculated.

2.7 Mechanical Characterization

3D printing provides different options for sample preperation. Test samples can be prepared in different orientations. Based on the previous literature[42], vertical X, Y–axis showed higher mechanical performance, therefore, all samples to be used in mechanical characterization processes were produced according to the vertical X, Y–axis configuration (Fig. S5). The tensile and impact strength tests of the 3D-printed nanocomposites were carried out in accordance with ASTM standards. Tensile tests of all samples were analyzed with Devotrans DVT model universal load frame at a speed of 5 mm/min in accordance with ASTM D 638 standard. Five samples were tested for neat ABS and MWCNT/ABS nanocomposites and average results were given. The Izod impact test was performed in accordance with ASTM D-256 standard according to the following parameters. The initial width of all samples was 10 mm and the tested width was taken as 8 mm since 2 mm was notched. The thickness was taken as 4 mm and the area of the samples subjected to the impact test was calculated as 32 mm^2. Five test samples were prepared for neat ABS and MWCNT/ABS nanocomposites. The average of the measurements was given as the test result.

2.8 Thermogravimetric Analysis

Thermogravimetric analysis (TGA) was performed on an EXSTAR S II 6300 TG/DTA apparatus with a heating rate of 10 °C/min from 30 to 700 °C under N_2 flow (20 ml/min).

3 Results and Discussion

The main goal of this study was to produce MWCNT/ABS functional nanocomposite filaments with improved mechanical and electrical properties that could be suitable candidates for the ESD application. The MWCNT/ABS nanocomposites with different nanofiller loadings (from 3 to 10 weight ratio) obtained by using a twin-screw extruder were converted into filament form with a diameter of 1.75 mm in a filament production line used in commercial production. In this study, ABS terpolymer was used as matrix due to its superior rheological, mechanical, and physical properties in FDM applications, whereas the MWCNT was chosen as the nanofiller, due to its higher aspect ratio as well as better mechanical and electrical properties. Since secondary interaction is high between nanotubes, generally they are found in the form aglomerates that looks like entangled spagetti. As given in Fig. S6, the agglomerate size and tube diameter of the neat MWCNT used in this study were determined as 11.72 µm and 37.5 nm, respectively.

Since printability is the most important criteria for FDM-based 3D printing process, MFI values of the MWCNT/ABS nanocomposites were firstly investigated to avoid nozzle clogging and formation of proper 3D geometry. Then, the distribution of nanofillers in the polymer matrix was examined by SEM analysis. Finally, the influence of nanofiller loadings on the 3D printing performance was also evaluated in terms of electrical, mechanical, and thermal properties.

3.1 Melt Flow Index (MFI) Analysis

The processibility and viscosity of MWCNT/ABS nanocomposites and neat ABS filaments were investigated by measuring MFI values. MFI values of the samples can be seen from Fig. 1, as a function of filler ratio. A significant decrease in MFI value occurred with the increase of MWCNT content. The neat ABS exhibited an MFI value of 38 g/10 min, whereas the MWCNT/ABS nanocomposite containing 3 wt% filler had an MFI value of 15 g/10 min. At the highest nanofiller content (C10-250 sample), MWCNT was responsible for the much higher MFI reduction, reaching the MFI values in the range of 0.5-2 g/10 min. The decrease % of MFI at 3, 5 and 10 wt% filler loading was calculated as 60.5, 94.7 and 98.7%, respectively. As obvious from the outcomes, the increase in the concentration of MWCNT led to a raise in the physical interactions between the MWCNT nanofiller and ABS matrix, which caused a high viscosity and a decrease in melt flow.[43] Also highly rigid structure of MWCNT should be considered that led to decrease in the flowability of the nanocomposites and increase the rigidity of the system in molten state.

3.2 Morphological Characterization

For the morphological analysis, the circular conductivity test samples were fractured, and their cross-sections were investigated by SEM analysis at different magnifications. The layered additive morphologies were seen from neat ABS and all nanocomposite samples regardless of the composition. In all cases, ABS was found as the continuous phase and acted as a binder between MWCNT nanofillers. As can be clearly seen in Figs. 2 and 3, neat ABS and MWCNT/ABS nanocomposite filaments were successfully employed with the FDM-type 3D printer under given conditions (Table 2). Parallel with the printing settings, all 3D printed samples showed almost no or very low volume voids

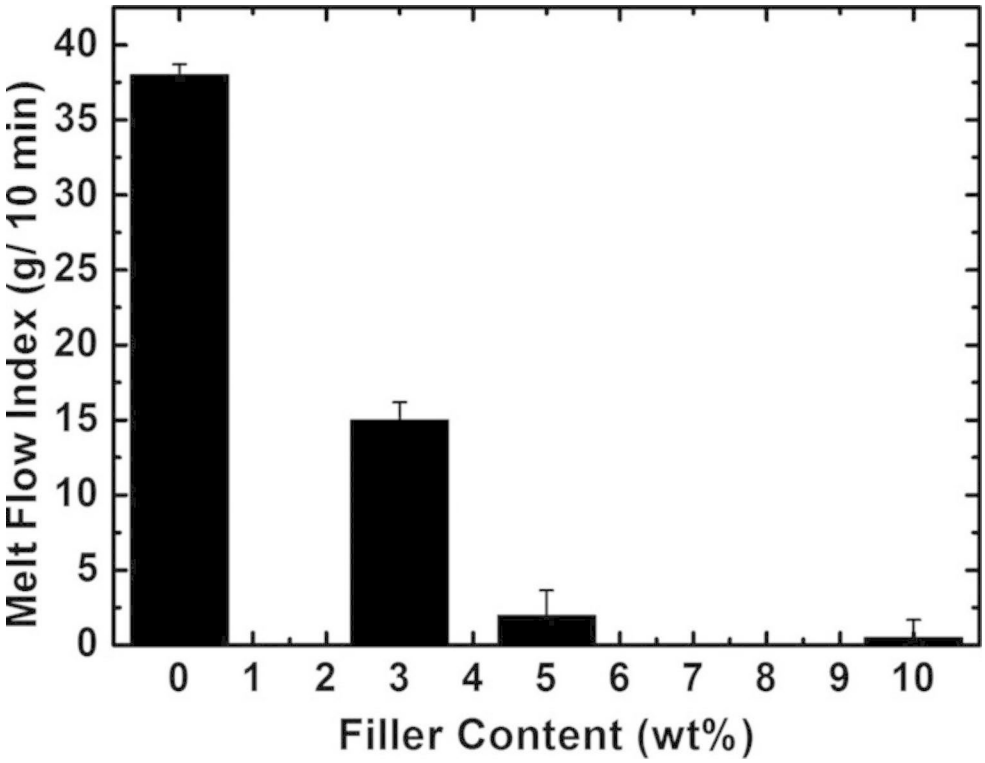

Fig. 1 The MFI values of neat ABS and MWCNT/ABS nanocomposite filaments

between layers, which was an indication of good layer-layer bonding and effective 3D printing.

To observe the morphology from micro to sub-micro scale, the SEM images of the printed samples were captured at various magnifications (Figs. 2, 3 and 4). Based on the SEM investigations, foam-like porous morphology was detected in all nanocomposite samples. This behavior was more dominant for C5-250 and C10-250 samples (Fig. 3). This might be due to nanofiller agglomeration at higher MWCNT loadings that was also reported previously for MWCNT/ABS nanocomposites [44]. As previously given in Fig. S6, although the average outer tube diameter was around 37.5 nm, the tubes formed relatively big agglomerates with an average size of around 11.72 µm. However, the average size of the agglomerate was found less than 1 µm for all 3D printed nanocomposite samples. That can be cross-checked from the Fig. 4, SEM images those have 1 µm scale bar. Even formation of the agglomerates were obvious, their size was lower than 1 µm and that is related with the mixing efficiency of the extruder. The average agglomerate size decreased from 11.72 µm to less than 1 µm. Since SEM analysis was performed by a random system, the resolution of the images was not good enough to calculate the actual average size of the agglomerates.

3.3 Characterization of Volume Resistivity

The main aim of this study was to reduce the electrical resistivity of 3D printed parts that could be suitable for ESD applications. In the literature, thermoplastics presenting ESD protection should have an electrical resistivity range between 10^6 and 10^{12} ohm.cm [45]. Since the 3D printing temperature directly affects the filler-matrix interactions (Table S1), melt rheology and the electrical properties of printed parts, the MWCNT/ABS nanocomposite containing 10 wt% nanofiller was printed at different temperatures (230, 250, 260, and 270 °C). The volume resistivity values of the obtained 3D printed samples were determined and the optimum 3D printing temperature was found as 250 °C in this study (Fig. 5a).

After determination of the optimum temperature, the volume resistivity values of all MWCNT/ABS nanocomposites were measured under similar conditions and their results were compared with the neat ABS sample (C0-250). As shown in Fig. 5b, the volume resistivity values of the C0-250, C3-250, C5-250 and C10-250 samples were found as 8.2E15, 3.96E15, 3.27E15, and 2.13E7 ohm.cm, respectively. The significant reduction in the volume resistivity of C10-250 could be due to the tunneling effect of the conductive network facilitated by the MWCNT nanofillers [45]. In this case, a high number of MWCNT connections could considerably reduce the tunneling distance where the electrons could tunnel from one MWCNT to another, thereby

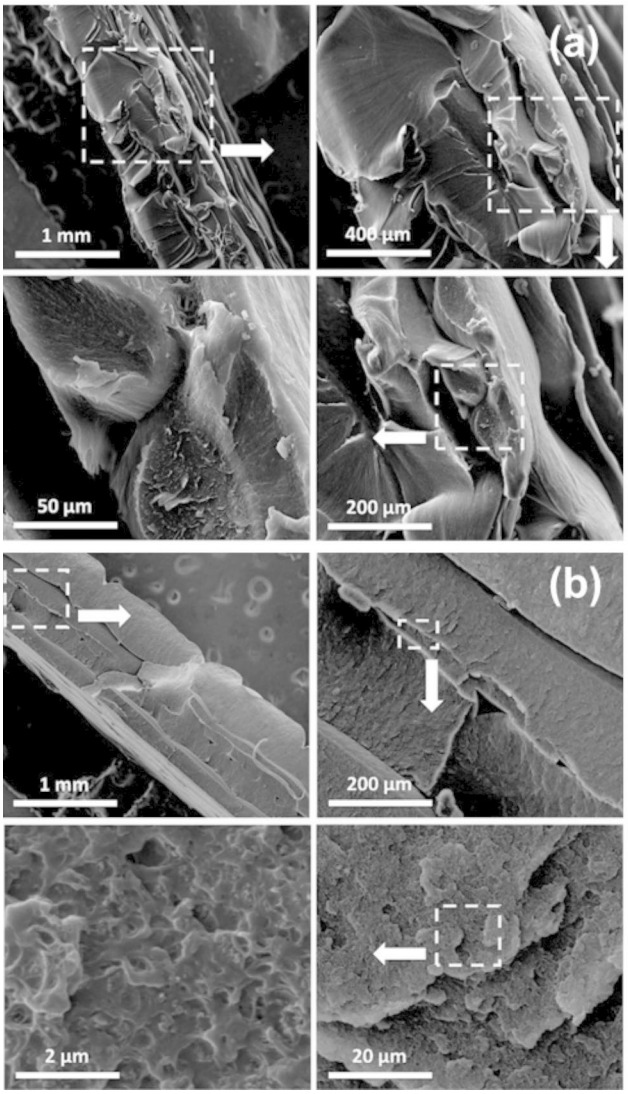

Fig. 2 SEM images of 3D printed C0-250 (neat ABS) (a) and C3-250 (nanocomposite) (b) at various magnifications

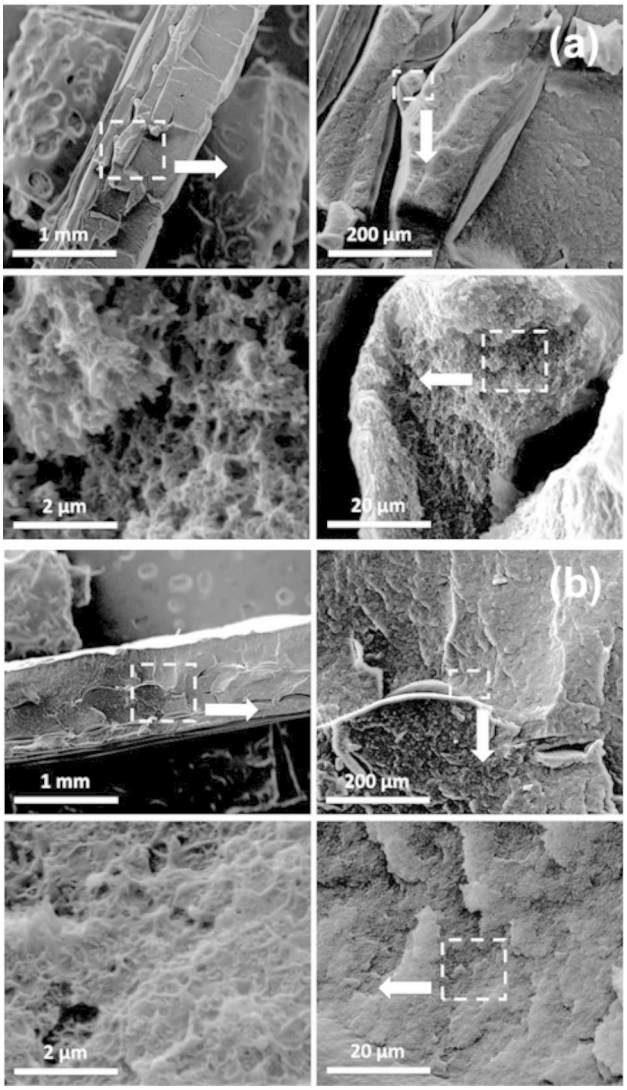

Fig. 3 SEM images of 3D printed C5-250 (a) and C10-250 nanocomposites (b) at various magnifications

defeating the high resistance of the ABS matrix [46]. This result was also supported by SEM analysis (Figs. 2, 3 and 4).

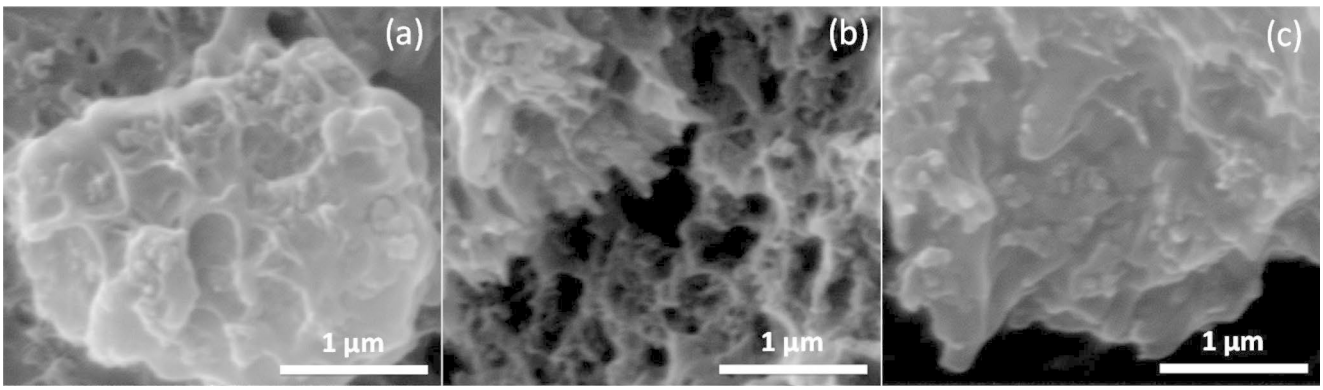

Fig. 4 SEM images of 3D printed C3-250 (a) C5-250 (b) and at 100k x magnification

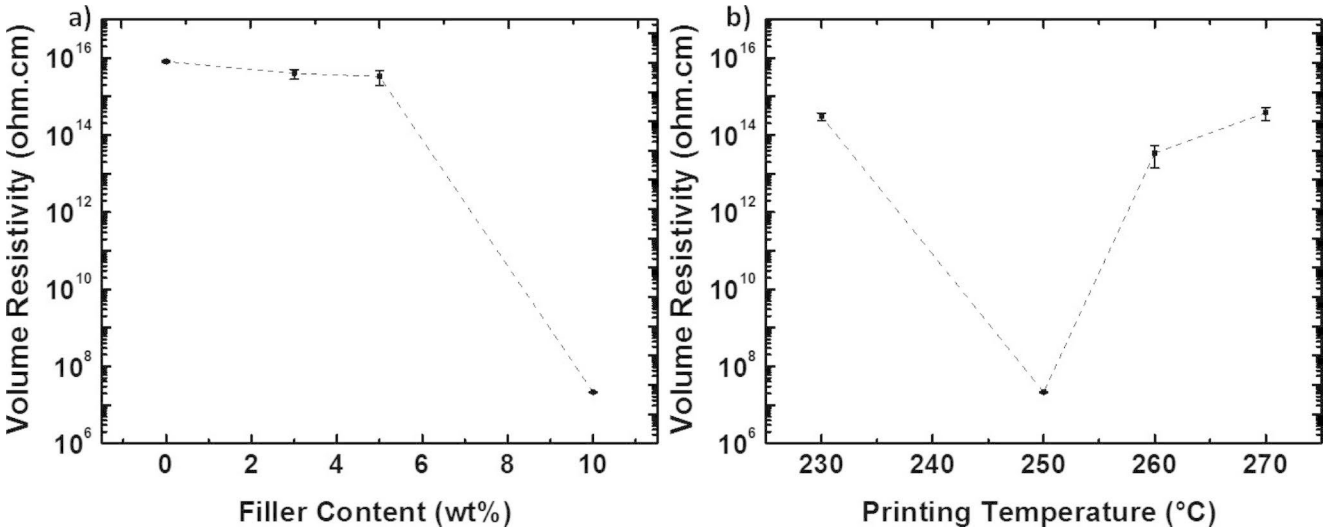

Fig. 5 Volume resistivity of samples as a function of filler content (a), volume resistivity of 10 wt% MWCNT filled ABS filament as a function of printing temperature (b)

As known, FDM type 3D printing is a process carried out in the molten phase of the thermoplastic polymers. Morphology, rheology, thermal stability of the polymer[44], CNT properties, processing conditions (speed, layer thickness, filling ratio, orientation of the rastering, printing temperature, cooling table temperature, cooling speed etc.), geometry, size of the sample, measurement system and standard method are of significance for electrical properties of the 3D printed samples (Table S1) [22, 28, 43, 47–51]. In all these, measurement system and standard method are very critical for obtaining accureate results. The system that consisted of an electode pair and high resistance meter are used for determination of volume resistivity and this reflects the bulk properties of the sample. However 2 or 4-probe systems are used to measure the surface/sheet resistance (R) and resistivity (σ) is calculated from the R, area (A) and length (l) values (σ = R*A/l) [52]. In that case it is assumed that sample is isotropic and current flow is same throughout the sample. In our case volume resistivity was measured by a system (Keithley 8009/ Keithley 6517B) based on ASTM D257 standard, that reflects the bulk property of the sample and can be different and/or lower compared to resistivity calculated from 2 or 4-probe resistance. As reported in the literature, the resistivity of the 3D printed samples are generally higher than injection molded samples and that was reported to be caused by high contact resistance between deposited layers [47]. Under that condition, polymer morphology, filler dispersion[44], 3D printing orientation and printing temperature are critical (Table S1). Polymer morphology is of significant not only for rheology and thermal degradation of the polymeric system but also for melting point. When ABS is considered, MWCNTs prefer to uniformly disperse in the styrene-acrylonitrile (SAN) phase. That behavior was attributed to non-covalent interactions of MWCNT and phenyl group of SAN in ABS [44]. At that point, even if mixing conditions were sufficient enough to disperse fillers, MWCNT can be mostly found in SAN phase as islands/sea and electron flow decreases. That behavior can lead to higher percolation concentrations as seen in MWCNT/ABS 3D printed [22, 28, 49].

In addition to these the orientation of 3D printing was reported to affect electrical properties of the samples. Orientation of the fillers can be affected by printing conditions such as speed and temperature. Based on the rastering speed, direction and temperature MWCNT-MWCNT network connection, MWCNT alignment, filling ratio and void volume can change [49]. So optimum temperature and orientation should be determined. In our case 250 °C was the optimum temperature for obtaining percolating network (Table S1). Below and above temperatures probably led to destruction of the conductive network [53]. Samples were printed in horizontal direction and further investigation is required in terms of optimum rastering direction.

3.4 Mechanical Characterization

Mechanical properties of the 3D printed MWCNT/ABS nanocomposites were investigated by tensile and impact tests and both test results were compared with the neat ABS sample under identical conditions (Fig. 6). Based on the tensile test results, the elastic modulus of the nanocomposites firstly increased from 375.05 to 576.71 MPa for the C3-250 sample, while these values decreased significantly to 461.82 and 441.88 MPa for the C5-250 and C10-250 nanocomposites due to the agglomeration of MWCNT nanofillers at higher loadings (Table 3) [54]. However, the C3-250,

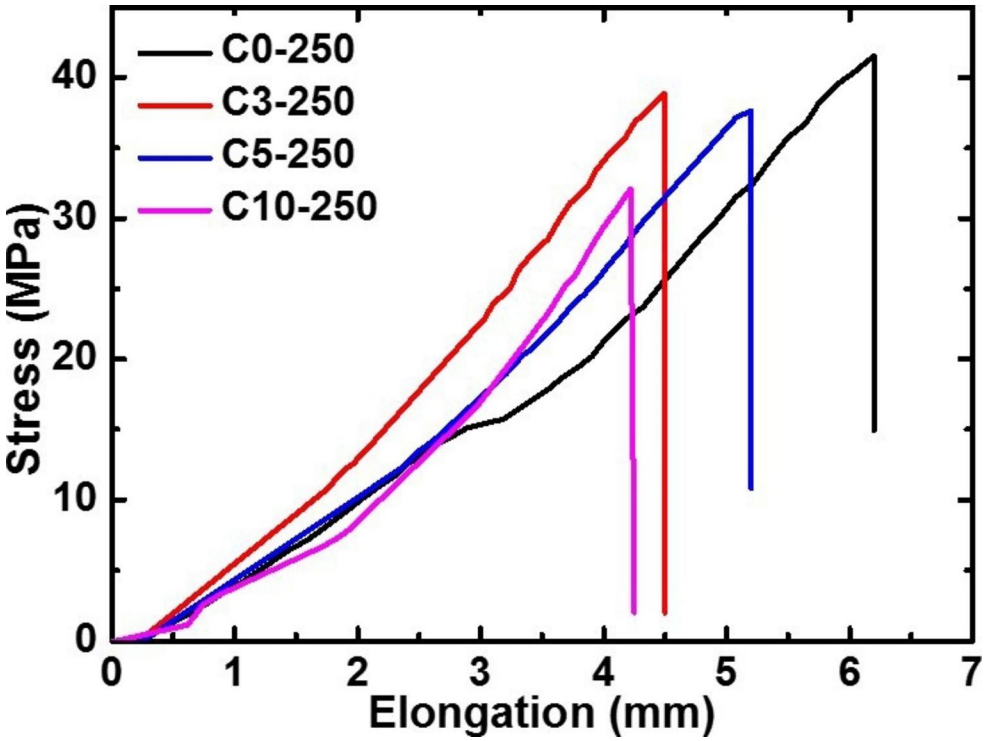

Fig. 6 Tensile test graph of 3D printed C0-250 (neat ABS), C3-250, C5-250 and C10-250 nanocomposites

Table 3 Summary of tensile test results of 3D printed the samples

Sample Code	Tensile stress (MPa)	Elongation at break (%)	Elastic modulus (MPa)
C0-250	41.55 ± 1.38	9.39 ± 0.87	375.03 ± 8.43
C3-250	38.84 ± 1.23	6.81 ± 0.65	576.71 ± 12.67
C5-250	37.62 ± 1.15	7.88 ± 0.54	461.82 ± 10.31
C10-250	32.10 ± 1.02	6.40 ± 0.42	441.88 ± 9.69

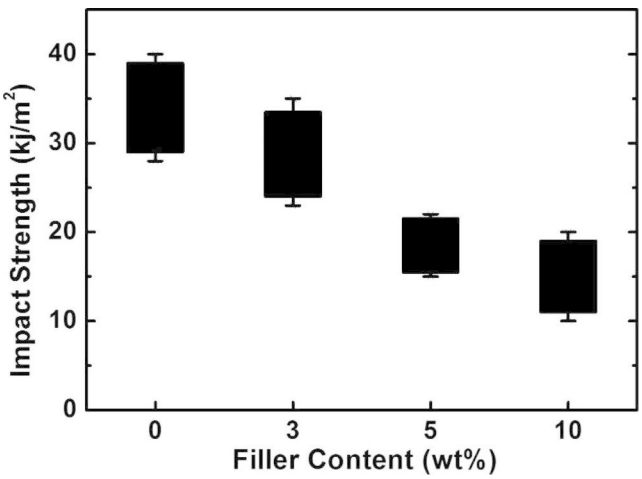

Fig. 7 Impact strengths of the samples as a function of filler content

C5-250, and C10-250 samples displayed 53.8, 23.1, and 17.8% higher elastic modulus compared to the neat ABS sample as the reference. On the other hand, the tensile stress and elongation at break values of the C3-250, C5-250, and C10-250 samples were slightly lower than those of the neat ABS sample. While the tensile stress values of neat ABS (CO-250) was determined as 41.55 MPa, these values of the C3-250, C5-250, and C10-250 nanocomposites were found as 38.84, 37.61, and 32.10 MPa, respectively. In addition, the elongation at break values of the C3-250, C5-250, and C10-250 nanocomposites were determined as 6.81, 7.88, and 6.40% were slightly lower than that of the neat ABS sample found as 9.39%. That decrease was probably due to nanofiller aggregations as given in the morphology section. The change in morphology and foam-like porous structure probably resulted in decreased resistance to stress.

The impact strength values of the MWCNT/ABS nanocomposites were also compared with that of neat ABS. It was noted that the impact strength of the neat ABS was higher than the corresponding nanocomposites (Fig. 7). By increasing the MWCNT content, the impact strength values of the nanocomposites were significantly decreased. The presence of MWCNT with 3 wt% in the ABS matrix reduced the impact resistance by approximately 25%. The reduced impact strength at higher nanofiller concentrations was due to the agglomerations of MWCNT nanotubes in the SAN phase [55]. Impact strength was generally expected to decrease with the incorporation of the rigid MWCNT into the tough polymers [56–59]. These findings were also consistent with morphology and tensile test results. Foam-like porous morphology was observed for nanocomposites when the filler content was higher, and the impact strengths of the 3D printed samples were sequentially decreased.

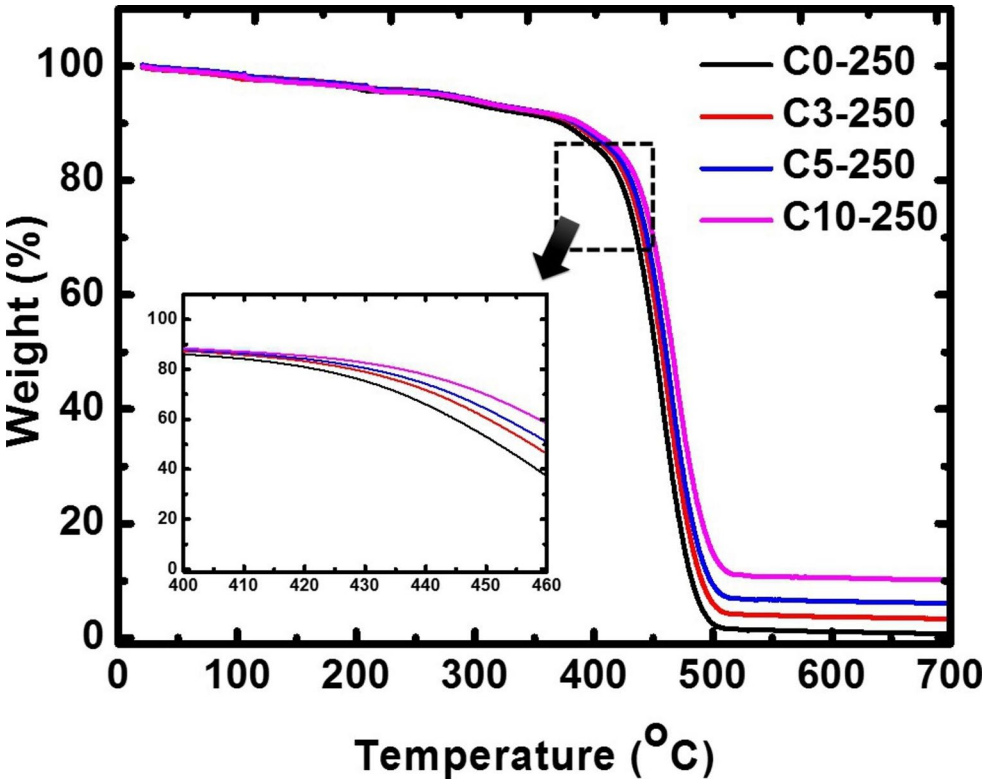

Fig. 8 TGA thermograms of 3D printed C0-250 (neat ABS), C3-250, C5-250 and C10-250 nanocomposites

Table 4 Thermal degradation behavior of the samples

Sample Code	$T_{10\%}$ (°C)	$T_{50\%}$ (°C)	Tmax (°C)	Char Yield wt% @ 700 °C
C0-250	373	452	458	0.70
C3-250	382	457	463	3.30
C5-250	385	460	465	6.03
C10-250	389	466	470	10.15

3.5 Thermogravimetric Analysis

Thermal properties of 3D printed MWCNT/ABS nanocomposite samples were compared with the neat ABS sample by thermogravimetric analysis under inert atmosphere with a heating rate of 10 °C/min from 30 to 700 °C. As shown in Fig. 8; Table 4, the neat ABS and MWCNT/ABS nanocomposites displayed a single degradation step between at 390 and 520 °C as similar to conventional vinyl polymers proceeding by random-chain and end-chain scissions [60]. The temperatures at 5% weight loss ($T_{5\%}$) and 50% weight loss ($T_{50\%}$), and char yields at 700 ºC were noted for neat ABS and 3D printed MWCNT/ABS nanocomposites. The increases in $T_{5\%}$, $T_{50\%}$, and char yields were determined by increasing MWCNT loading. The $T_{5\%}/T_{50\%}$, and char yield % of neat ABS were found as 322.60, 452.77 °C, and 0.65%, whereas these values were 362.38/467.47 °C and 11.16% for the nanocomposite containing the highest MWCNT loading (C10-250). The incorporation of MWCNT in the ABS matrix led to restrict the segmental movements of polymer chains enabling to enhance the thermal properties of resulting 3D printed MWCNT/ABS nanocomposites.

4 Conclusion

In conclusion, the MWCNT/ABS nanocomposite filaments with the filler content of 3, 5, and 10 wt% were successfully prepared by a specially designed extruder for the FDM-type 3D printing. Then, these nanocomposites were readily converted into monofilament forms used in the FDM-type 3D printers to produce test samples to reveal their morphological, mechanical, and electrical properties for the potential ESD application. By the addition of MWCNT into the ABS matrix led to a raise physical interactions that caused a high viscosity and a decrease in melt flow. Based on the morphological analysis, foam-like porous morphology that directly affected the conductivity and mechanical properties of the nanocomposites was detected. With the addition of MWCNT nanofiller, the tensile modulus and thermal properties of the 3D printed samples were significantly improved, but the elongation at break and impact strength values were notably decreased. As a result of the volume resistivity test, the 3D printing temperature and content of MWCNT were optimized and the optimum values were found as 250 ºC and 10 wt% respectively. The obtained sample displayed the lowest volume resistivity as 2.13E7 ohm.cm, which fulfills the requirement of the ESD protection.

Supplementary Information The online version contains supplementary material available at https://doi.org/10.1007/s42250-022-00469-3.

Declarations

Conflict of Interest The authors have no confict of interest to disclose.

Competing Interests The authors declare that they have no known competing financial interests or personal relationships that could have appeared to influence the work reported in this paper.

References

1. Campbell TA, Ivanova OS (2013) 3D printing of multifunctional nanocomposites. Nano Today 8:119–120
2. Jandyal A, Chaturvedi I, Wazir I, Raina A, Haq MIU (2022) 3D printing–A review of processes, materials and applications in industry 4.0. Sustainable Oper Comput 3:33–42
3. Zhang J, Yang B, Fu F, You F, Dong X, Dai M (2017) Resistivity and its anisotropy characterization of 3D-printed acrylonitrile butadiene styrene copolymer (ABS)/carbon black (CB) composites. Appl Sci 7:20
4. Winder J, Bibb R (2005) Medical rapid prototyping technologies: state of the art and current limitations for application in oral and maxillofacial surgery. J Oral Maxillofac Surg 63:1006–1015
5. Youssef A, Hollister SJ, Dalton PD (2017) Additive manufacturing of polymer melts for implantable medical devices and scaffolds. Biofabrication 9:012002
6. Ackland DC, Robinson D, Redhead M, Lee PVS, Moskaljuk A, Dimitroulis G (2017) A personalized 3D-printed prosthetic joint replacement for the human temporomandibular joint: From implant design to implantation. J Mech Behav Biomed Mater 69:404–411
7. Yap YL, Yeong WY (2014) Additive manufacture of fashion and jewellery products: a mini review. Virtual Phys Prototyping 9:195–201
8. Camacho DD, Clayton P, O'Brien WJ, Seepersad C, Juenger M, Ferron R, Salamone S (2018) Applications of additive manufacturing in the construction industry–A forward-looking review. Autom Constr 89:110–119
9. Moon SK, Tan YE, Hwang J, Yoon Y-J (2014) Application of 3D printing technology for designing light-weight unmanned aerial vehicle wing structures. Int J Precis Eng Manuf 1:223–228
10. Podsiadły B, Skalski A, Wałpuski B, Słoma M (2019) Heterophase materials for fused filament fabrication of structural electronics. J Mater Sci : Mater Electron 30:1236–1245
11. Berman B (2012) 3-D printing: The new industrial revolution. Bus Horiz 55:155–162
12. Bourell D, Kruth JP, Leu M, Levy G, Rosen D, Beese AM, Clare A (2017) Materials for additive manufacturing. CIRP Ann 66:659–681
13. Abeykoon C, Sri-Amphorn P, Fernando A (2020) Optimization of fused deposition modeling parameters for improved PLA and ABS 3D printed structures. Int J Lightweight Mater Manuf 3:284–297
14. Wang P, Zou B, Xiao H, Ding S, Huang C (2019) Effects of printing parameters of fused deposition modeling on mechanical properties, surface quality, and microstructure of PEEK. J Mater Process Technol 271:62–74
15. Gebisa AW, Lemu HG (2018) Investigating effects of fused-deposition modeling (FDM) processing parameters on flexural properties of ULTEM 9085 using designed experiment. Materials 11:500
16. Saenz F, Otarola C, Valladares K, Rojas J (2021) Influence of 3D printing settings on mechanical properties of ABS at room temperature and 77 K. Addit Manuf 39:101841
17. Park S, Shou W, Makatura L, Matusik W, Fu KK (2022) 3D printing of polymer composites: Materials, processes, and applications. Matter 5:43–76
18. Azlin MNM, Ilyas RA, Zuhri MYM, Sapuan SM, Harussani MM, Sharma S, Nordin AH, Nurazzi NM, Afiqah AN (2022) 3D printing and shaping polymers, composites, and nanocomposites: a review. Polymers 14:180
19. Tekinalp HL, Kunc V, Velez-Garcia GM, Duty CE, Love LJ, Naskar AK, Blue CA, Ozcan S (2014) Highly oriented carbon fiber–polymer composites via additive manufacturing. Compos Sci Technol 105:144–150
20. Shofner ML, Lozano K, Rodríguez-Macías FJ, Barrera EV (2003) Nanofiber-reinforced polymers prepared by fused deposition modeling. J Appl Polym Sci 89:3081–3090
21. Zhong W, Li F, Zhang Z, Song L, Li Z (2001) Short fiber reinforced composites for fused deposition modeling. Mater Sci Eng A 301:125–130
22. Vidakis N, Maniadi A, Petousis M, Vamvakaki M, Kenanakis G, Koudoumas E (2020) Mechanical and electrical properties investigation of 3D-printed acrylonitrile–butadiene–styrene graphene and carbon nanocomposites. J Mater Eng Perform 29:1909–1918
23. Vidakis N, Petousis M, Tzounis L, Velidakis E, Mountakis N, Grammatikos SA (2021) Polyamide 12/multiwalled carbon nanotube and carbon black nanocomposites manufactured by 3D printing fused filament fabrication: A comparison of the electrical, thermoelectric, and mechanical properties. J Carbon Res 7:38
24. Le T-H, Le V-S, Dang Q-K, Nguyen M-T, Le T-K, Bui N-T (2021) Microstructure evaluation and thermal–mechanical properties of abs matrix composite filament reinforced with multi-walled carbon nanotubes by a single screw extruder for fdm 3d printing. Appl Sci 11:8798
25. Sezer HK, Eren O (2019) FDM 3D printing of MWCNT reinforced ABS nano-composite parts with enhanced mechanical and electrical properties. J Manuf Processes 37:339–347
26. Zuikafly SNF, Ahmad F, Ibrahim MH, Latif AA, Harun SW (2017) Demonstration of passive saturable absorber by utilizing MWCNT-ABS filament as starting material. IOP Conference Series: Materials Science and Engineering 210:012030
27. Vidakis N, Petousis M, Kourinou M, Velidakis E, Mountakis N, Fischer-Griffiths PE, Grammatikos S, Tzounis L (2021) Additive manufacturing of multifunctional polylactic acid (PLA)—multiwalled carbon nanotubes (MWCNTs) nanocomposites. Nanocomposites 7:184–199
28. Dul S, Gutierrez BJA, Pegoretti A, Alvarez-Quintana J, Fambri L (2022) 3D printing of ABS Nanocomposites. Comparison of processing and effects of multi-wall and single-wall carbon nanotubes on thermal, mechanical and electrical properties. J Mater Sci Technol 121:52–66
29. Ambrosi A, Pumera M (2016) 3D-printing technologies for electrochemical applications. Chem Soc Rev 45:2740–2755
30. Ambrosi A, Moo JGS, Pumera M (2016) Helical 3D-printed metal electrodes as custom-shaped 3D platform for electrochemical devices. Adv Funct Mater 26:698–703
31. Kong YL, Tamargo IA, Kim H, Johnson BN, Gupta MK, Koh T-W, Chin H-A, Steingart DA, Rand BP, McAlpine MC (2014) 3D printed quantum dot light-emitting diodes. Nano Lett 14:7017–7023
32. Verma S, Dhangar M, Mili M, Bajpai H, Dwivedi U, Kumari N, Khan MA, Bhargaw HN, Hashmi SAR, Srivastava AK (2022) Review on engineering designing of electromagnetic interference

shielding materials using additive manufacturing. Polym. Compos
33. Dul S, Fambri L, Pegoretti A (2016) Fused deposition modelling with ABS–graphene nanocomposites. Compos Part A 85:181–191
34. Jakus AE, Secor EB, Rutz AL, Jordan SW, Hersam MC, Shah RN (2015) Three-dimensional printing of high-content graphene scaffolds for electronic and biomedical applications. ACS Nano 9:4636–4648
35. Zhang Q, Zhang F, Medarametla SP, Li H, Zhou C, Lin D (2016) 3D printing of graphene aerogels. Small 12:1702–1708
36. Wei X, Li D, Jiang W, Gu Z, Wang X, Zhang Z, Sun Z (2015) 3D printable graphene composite. Sci Rep 5:1–7
37. Byrne EM, McCarthy MA, Xia Z, Curtin WA (2009) Multi-wall Nanotubes Can Be Stronger than Single Wall Nanotubes and Implications for Nanocomposite Design. Phys Rev Lett 103:045502
38. Junpha J, Wisitsoraat A, Prathumwan R, Chaengsawang W, Khomungkhun K, Subannajui K (2020) Electronic tongue and cyclic voltammetric sensors based on carbon nanotube/polylactic composites fabricated by fused deposition modelling 3D printing. Mater Sci Eng C 117:111319
39. Gnanasekaran K, Heijmans T, Van Bennekom S, Woldhuis H, Wijnia S, De With G, Friedrich H (2017) 3D printing of CNT-and graphene-based conductive polymer nanocomposites by fused deposition modeling. Appl Mater Today 9:21–28
40. Tambrallimath V, Keshavamurthy R, Saravanabavan D, Koppad PG, Sethuram D (2020) Mechanical Characterization of PC-ABS Reinforced with CNT Nanocomposites developed by Fused Deposition Modelling. J Phys Conf Ser 1455:012003
41. Lubombo C, Huneault MA (2018) Effect of infill patterns on the mechanical performance of lightweight 3D-printed cellular PLA parts. Mater Today Commun 17:214–228
42. Zhang H, Cai L, Golub M, Zhang Y, Yang X, Schlarman K, Zhang J (2018) Tensile, creep, and fatigue behaviors of 3D-printed acrylonitrile butadiene styrene. J Mater Eng Perform 27:57–62
43. Dul S, Fambri L, Pegoretti A (2018) Filaments production and fused deposition modelling of ABS/carbon nanotubes composites. Nanomaterials 8:49
44. Waheed Q, Khan AN, Jan R (2016) Investigating the reinforcement effect of few layer graphene and multi-walled carbon nanotubes in acrylonitrile-butadiene-styrene. Polymer 97:496–503
45. Arigbabowo OK, Tate JS (2021) Additive manufacturing of polyamide nanocomposites for electrostatic charge dissipation applications. Mater Sci Eng B 271:115251
46. Podsiadły B, Matuszewski P, Skalski A, Słoma M (2021) Carbon nanotube-based composite filaments for 3d printing of structural and conductive elements. Appl Sci 11:1272
47. Dorigato A, Moretti V, Dul S, Unterberger SH, Pegoretti A (2017) Electrically conductive nanocomposites for fused deposition modelling. Synth Met 226:7–14
48. Horst JD, De Andrade PP, Duvoisin CA, Vieira RD (2020) Fabrication of conductive filaments for 3D-printing: Polymer nanocomposites. Biointerface Res Appl Chem 10:6577–6586
49. Thaler D, Aliheidari N, Ameli A (2019) Mechanical, electrical, and piezoresistivity behaviors of additively manufactured acrylonitrile butadiene styrene/carbon nanotube nanocomposites. Smart Mater Struct 28:084004
50. Schmitz DP, Ecco LG, Dul S, Pereira ECL, Soares BG, Barra GMO, Pegoretti A (2018) Electromagnetic interference shielding effectiveness of ABS carbon-based composites manufactured via fused deposition modelling. Mater Today Commun 15:70–80
51. Schmitz DP, Dul S, Ramoa S, Soares BG, Barra GMO, Pegoretti A (2021) Effect of printing parameters on the electromagnetic shielding efficiency of ABS/carbonaceous-filler composites manufactured via filament fused fabrication. J Manuf Processes 65:12–19
52. Cetin MS, Toprakci HAK (2021) Flexible electronics from hybrid nanocomposites and their application as piezoresistive strain sensors. Compos Part B 224:109199
53. Fernandes JPC, Castro LDC, Mareau VH, Pessan LA, Gonon L (2018) New insights on the compatibilization of PA6/ABS blends: A co-localized AFM-Raman study. Polymer 146:151–160
54. Fayazbakhsh K, Movahedi M, Kalman J (2019) The impact of defects on tensile properties of 3D printed parts manufactured by fused filament fabrication. Mater Today Commun 18:140–148
55. Mousavi MR, Tehran AC, Shelesh-Nezhad K (2020) Study on morphology, mechanical, thermal and viscoelastic properties of PA6/TPU/CNT nanocomposites. Plast. Rubber Compos 49:400–413
56. Jindal P, Jyoti J, Kumar N (2016) Mechanical characterisation of ABS/MWCNT composites under static and dynamic loading conditions. J Mech Eng Sci 10:2288–2299
57. Pour RH, Hassan A, Soheilmoghaddam M, Bidsorkhi HC (2016) Mechanical, thermal, and morphological properties of graphene reinforced polycarbonate/acrylonitrile butadiene styrene nanocomposites. Polym Compos 37:1633–1640
58. Jiang X, Drzal LT (2010) Multifunctional high density polyethylene nanocomposites produced by incorporation of exfoliated graphite nanoplatelets 1: morphology and mechanical properties. Polym Compos 31:1091–1098
59. Wakabayashi K, Pierre C, Dikin DA, Ruoff RS, Ramanathan T, Brinson LC, Torkelson JM (2008) Polymer – graphite nanocomposites: effective dispersion and major property enhancement via solid-state shear pulverization. Macromolecules 41:1905–1908
60. Balart R, Garcia-Sanoguera D, Quiles-Carrillo L, Montanes N, Torres-Giner S (2019) Kinetic analysis of the thermal degradation of recycled acrylonitrile-butadiene-styrene by non-isothermal thermogravimetry. Polymers 11:281